Identifying alternative ferroelectric materials beyond Hf(Zr)O₂

Cite as: Appl. Phys. Lett. **117**, 262903 (2020); https://doi.org/10.1063/5.0028611 Submitted: 05 September 2020 . Accepted: 11 December 2020 . Published Online: 28 December 2020

🗓 Jing Guo, 🗓 Sergiu Clima, 🗓 Geoffrey Pourtois, and 🗓 Jan Van Houdt

COLLECTIONS

Paper published as part of the special topic on Ferroelectricity in Hafnium Oxide: Materials and Devices







ARTICLES YOU MAY BE INTERESTED IN

Polarization switching in thin doped HfO₂ ferroelectric layers

Applied Physics Letters 117, 262904 (2020); https://doi.org/10.1063/5.0035100

Quantifying non-centrosymmetric orthorhombic phase fraction in 10 nm ferroelectric $Hf_{0.5}Zr_{0.5}O_2$ films

Applied Physics Letters 117, 262905 (2020); https://doi.org/10.1063/5.0029611

Impact of the SiO₂ interface layer on the crystallographic texture of ferroelectric hafnium oxide

Applied Physics Letters 118, 012901 (2021); https://doi.org/10.1063/5.0029635





Identifying alternative ferroelectric materials beyond Hf(Zr)O₂

Cite as: Appl. Phys. Lett. 117, 262903 (2020); doi: 10.1063/5.0028611 Submitted: 5 September 2020 · Accepted: 11 December 2020 · Published Online: 28 December 2020













AFFILIATIONS

¹Department of Electrical and Computer Engineering, University of Florida, Gainesville, Florida 32611, USA

Note: This paper is part of the Special Topic on Materials and Devices Utilizing Ferroelectricity in Halfnium Oxide.

^{a)}Author to whom correspondence should be addressed: guoj@ufl.edu

ABSTRACT

A database-driven approach combined with ab initio density functional theory (DFT) simulations is used to identify and simulate alternative ferroelectric materials beyond Hf(Zr)O2. The database-driven screening method identifies a class of wurtzite ferroelectric materials. DFT simulations of wurtzite magnesium chalcogenides, including MgS, MgSe, and MgTe, show their potential to achieve improved ferroelectric (FE) stability, simple atomistic unit cell structure, and large FE polarization. Strain engineering can effectively modulate the FE switching barrier height for facilitating FE switching. The effect of the piezoelectric property on the FE switching barrier heights is also examined.

Published under license by AIP Publishing. https://doi.org/10.1063/5.0028611

Ferroelectric (FE) materials have extensive applications in modern nonvolatile memory technologies, RF switches, actuators, and sensors. Compared to perovskite ferroelectric materials, HfO2 and HfZrO_x(HZO)-based ferroelectric materials enjoy excellent compatibility with the CMOS process and have been investigated as ferroelectric memory material for the last decade or so. While the HfO2 ferroelectric materials have attractive properties, certain drawbacks, such as stability of the ferroelectric phase and difficulty to maintain low leakage and ferroelectricity for ultrathin films, limit their potential for applications. Identifying alternative ferroelectric materials beyond HfO2 and HZO that can address these limitations is called for. In this Letter, we report a group of binary ferroelectric materials beyond HfO₂ and HZO, identified by a database-driven screening approach. *Ab initio* density functional theory (DFT) simulations are subsequently applied to calculate the ferroelectric material properties of the wurtzite class of identified FE materials.

We first examine the features and limitations of the Hf(Zr)O₂ ferroelectric materials. A methodology to screen and identify alternative FE materials is discussed next. Finally, the ferroelectric properties of several identified binary wurtzite magnesium chalcogenide materials are investigated and benchmarked. The materials identified here are beyond the FE material candidates suggested in previous studies.^{2,3} Furthermore, important material properties, including the FE switching barrier height, FE stability, and material structural simplicity, are investigated in the material selection process.

To calculate the ferroelectric material properties, ab initio density functional theory simulations were performed. The ferroelectric material properties of the wurtzite phase magnesium chalcogenides are calculated by using the Vienna ab initio simulation package (VASP) codes.⁴ The calculation was performed by using the projector augmented-wave (PAW) pseudopotential, and the generalized gradient approximation (GGA) method was used with a Perdew-Burke-Ernzerhof (PBE) exchange-correlation functional. The Brillouin zone was sampled by a $6 \times 6 \times 6$ Monkhorst-Pack scheme. The ferroelectric polarization is calculated by using the Berry phase theory. The cutoff energy for the wave-function expansion is set to 600 eV. Nudged elastic band (NEB) simulations are used to determine the ferroelectric switching barrier height.

Both HfO2 and HZO have a rich set of crystalline phases, and only a small fraction of phases are ferroelectric. Out of dozens of possible crystalline phases, only three have been shown to be ferroelectric, which include orthorhombic $Pca2_1$, $Pmn2_1$, ⁶ and rhombohedral R3mphases. Furthermore, the antiferroelectric characteristics of HfO₂ are attributed to the tetragonal P42/nmc phase.8 In addition, there is one case of the Pbca systems that has two anti-aligned polarization unit cells of Pca21, which could also form an antiferroelectric material

²IMEC, Kapeldreef 75, 3001 Heverlee, Belgium

³PLASMANT, University of Antwerp, 2610 Antwerpen, Belgium

ESAT, KU Leuven, 3001 Leuven, Belgium

system. In HfO₂ and HZO, the *Pca2₁* phase is postulated to be the ferroelectric phase in technologically relevant applications. At the atomic level, there are at least 6 possible atomic pathways for the polarization reversal mechanism. However, only one of them, which switches through the *Pbcm* phase, aligns the electric dipoles to the applied electric field and reduces the potential energy, as shown in Figs. 1(a) and 1(b). Figure 1(c) shows the atomic structures of this pathway in the FE switching process. Five other mechanisms imply an antialignment of the electric dipoles with the electric field, which does not correspond to the definition of the ferroelectric switching. However, all these mechanisms are still relevant for the material breakdown. These mechanisms can follow the first electric switching event at very high electric fields or in the wakeup/fatigue regimes, where the crystalline phase transforms into non-ferroelectric phases.

Because in HfO₂ and ZrO₂, many other phases are more stable than the FE phases, achieving the FE phases requires special processing for stabilization. ¹² Strain, special thermal treatments, and doping have been used to stabilize the ferroelectric phases. For example, in terms of doping, one can use dopants including Si, Al, Y, La, or Gd to stabilize the FE phase. The extrinsic dopant atoms, even in relatively low percentage, can result in local strain, so that further local atomic rearrangement toward the most stable monoclinic phase is delayed. This effect is beneficial for stabilizing the ferroelectric phase. ¹³ However, the presence of strain at the material interfaces and grain boundaries can result in lattice deformation and impact the energy stabilization of phase transformation. Furthermore, the piezoelectric response of the materials due to the applied electric field can result in additional lattice deformation with an applied electric field in HfO₂ and HZO.

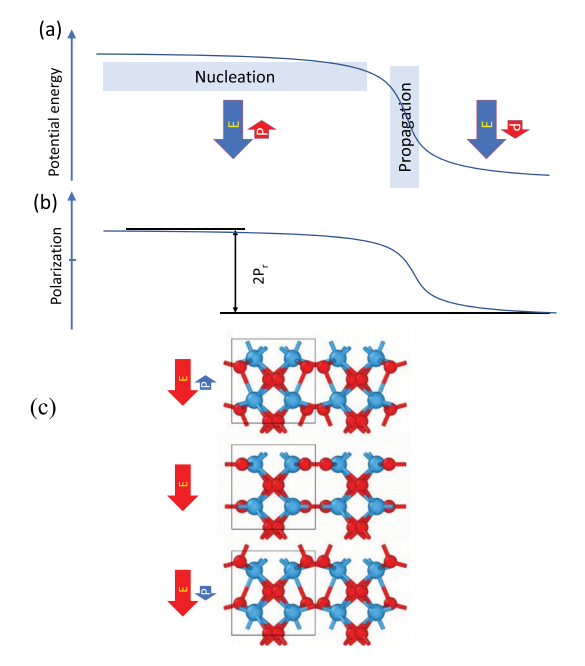


FIG. 1. (a) Schematic evolution of the potential energy during the polarization reversal process in a configuration with the starting negative field, positive polarization. (b) FE polarization evolves with the negative slope during the propagation phase, therefore aligning with the electric field. (c) Atomic pathway for polarization reversal in the FE switching process of HfO₂. The directions of the electric field and polarization are denoted as E and P, respectively.

In order to examine the stability of the FE phase with the deformation of the lattice parameters, Fig. 2 plots the simulation results of the potential energy surface by scanning the unit cell lattice parameters in the simulation. Instead of observing one basin feature typical to one phase, the results indicate two basins with a small energy potential barrier between them, upon changing the unit cell length parameters. As shown in the figure, one basin corresponds to the FE phase and the other corresponds to a non-FE phase. As shown in Fig. 2, Hf(Zr)O_x does not have large kinetic barriers to lose the ferroelectric phase, and there are rich features in potential energy surface. As a result, a small strain relaxation can push relatively easy the FE phase into another (non-FE) phase. At certain applied strain, the barrier for phase transformation is small at 20-40 meV/atom, which is comparable to or below the polarization switching barrier of 100-200 meV/switching atom. 9,10 It has also been previously shown that in FE Hf(Zr)Ox, the phase transformation and polarization rotation barriers are low and strain relaxation can lead to phase transformation. 14,15

Due to these limitations, it is desirable to have alternative ferroelectric material choices beyond Hf(Zr)O_x. Hence, to find alternative materials, we employed a systematic database-driven screening approach as outlined in Fig. 3. The procedure screens ~125000 structures available in the Materials Project Database (materialsproject.org). 16 Among the materials screened, the following criteria are imposed to identify the FE materials of interest: (i) the FE materials belong to non-centrosymmetric polar lattice space groups; (ii) the semiconductor fabrication process requires certain elements to be excluded, which includes those in the first and seventh columns of the period table, Pb and Cd, radioactive elements, and Actinides; (iii) the energy above Hull, which is defined as the energy above the most stable (i.e., lowest-energy) crystalline phase at the same chemical composition, is required to be <50 meV for stability of the FE phase; in comparison, ferroelectric HfO2 has an energy above Hull of 29 meV; (iv) the energy bandgap, which is computed by the DFT calculations with the bandgap underestimation problem, is required to be larger than 2.3 eV. A larger bandgap makes a material closer to an insulator and leads to a larger barrier and lower intrinsic leakage current. In comparison, FE BaTiO₃ has a bandgap of 2.56 eV in the trigonal phase and a bandgap of 2.3 eV in the orthorhombic phase. The value of

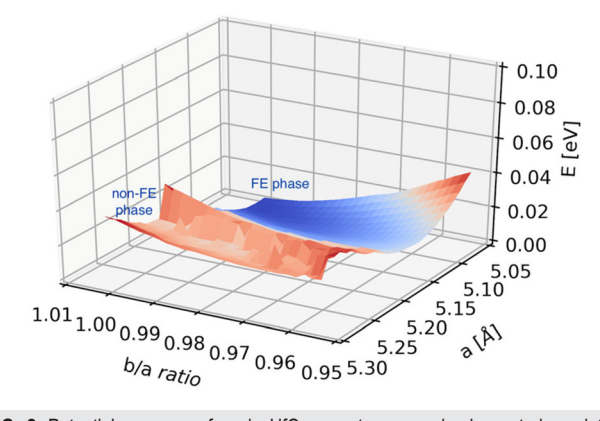


FIG. 2. Potential energy surface in HfO_2 per atom upon in-plane strain variation (polarization along the out-of-plane b axis, a/c is fixed, and b/a and a are varying) for a window of a between 5.05 and 5.30 Å and the b/a ratio between 0.96 and 1.01

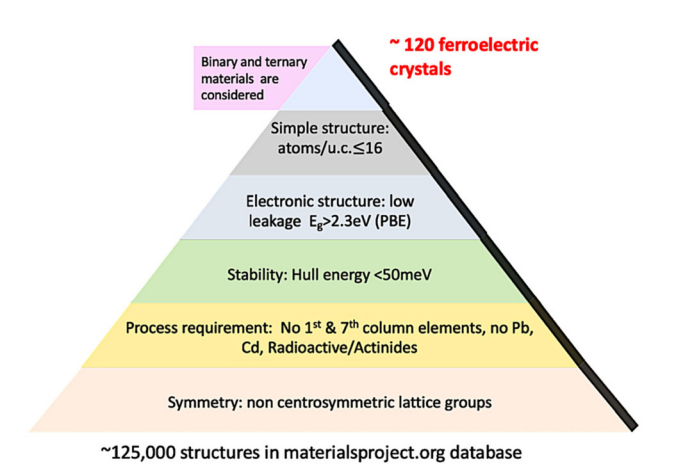


FIG. 3. FE material down selection methodology: The selection criteria are shown, which identifies \sim 120 FE candidates out of \sim 125 000 structures in the material-sproject.org database.

 $2.3\,\mathrm{eV}$ ensures that $\mathrm{BaTiO_3}$, which is a known FE material, meets the criterion. It is, however, not a sufficient condition for guaranteeing small leakage, especially if the coercive field of a candidate FE material is considerably larger than that of $\mathrm{BaTiO_3}$; (v) the unit cell structure needs to be simple enough, so that the number of sites per unit cell is ≤ 16 , which is preferred for ease of material synthesis and fabrication; and (vi) only binary and ternary FE materials are searched for simplicity.

Applying the above database screening criteria, we found 120 candidates out of ~125 000 structures screened, which are shown in Fig. 4. Each material is represented by a labeled data point in the bandgap vs the energy above the Hull plot. The FE material selection process described above identifies the common FE materials including BaTiO₃, HfO₂, and ZrO₂, which are highlighted in the plot. Furthermore, a class of Wurtzite lattice materials in the space group P6₃mc are identified as candidate FE materials, which include (i) BeO; (ii) Nitride materials, AlN, BN, and AlGaN2; and (iii) wurtzite magnesium chalcogenides, including MgS, MgSe, and MgTe. Because Be and its compound shall be avoided in the semiconductor process due to health-hazardous consideration and BeO has an excessively high switching barrier, it is not further investigated. For nitride materials, it has been demonstrated that Sc doping can result in ferroelectric Nitride material based on AlN. 17 For magnesium chalcogenides, MgS, MgSe, and MgTe, identified from the database-driven screening procedure, are highlighted in Fig. 4. These wurtzite lattice materials have the

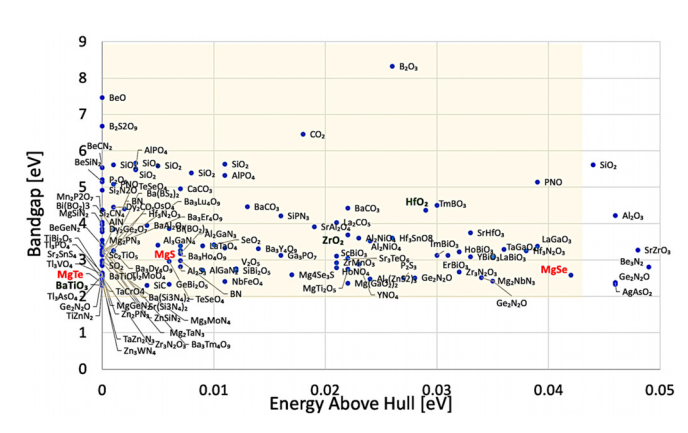


FIG. 4. The material bandgap vs energy above Hull for the candidate FE materials coming out from the down selection methodology as shown in Fig. 3. Each data point denotes a candidate material. The area of interest is highlighted, which has a bandgap larger than that of BaTiO $_3$ and the energy above Hull smaller than that of ferroelectric HfO $_2$.

feature of a simple unit cell structure with a small number of sites per unit cell, which is advantageous for simplifying material synthesis, and they are further investigated by using DFT simulations.

The stability of the wurtzite phase can be assessed from its energy above the Hull and number of competing phases. The identified phase of wurtzite MgS (w-MgS) belongs to the hexagonal space group P63mc, whose energy is 7 meV above the lowest phase in the cubic space group $Fm\overline{3}m$, which is the only phase with lower energy than the FE phase. For wurtzite MgSe (w-MgSe), in the space group, P63mc is 42 meV above the lowest crystalline phase, and there are two phases with energies lower than the FE $P6_3mc$ phase (i.e., the cubic $F\overline{4}3m$ and Fm3m phases). For wurtzite MgTe (w-MgTe), the wurtzite phase is the lowest energy phase. In comparison, as shown in Table I, the FE phase of HfO₂ is 29 meV above the lowest phase with a monoclinic lattice, and there are at least 5 phases (i.e., P2₁/c, Pbca1, Pbca2, P4₂/mnm, and Pbcn) with energy lower than the FE phase. Therefore, compared to FE HfO2, the wurtzite phase of MgS and MgTe is energetically more stable and preferred over other crystalline phases, with one or zero competing lower-energy phases, respectively. Despite of higher energy above Hull for w-MgSe, it has a smaller number of two competing non-ferroelectric crystalline phases.

The ferroelectric polarization and switching barrier properties are examined next. Figure 5 shows the simulated energy per switching atom or formula unit (f.u.) as a function of ferroelectric polarization in

TABLE I. Comparison of material properties between HfO2, MgS, MgSe, and MgTe. Bandgap values are from the materialsproject.org database, which is computed with GGA.

	HfO_2	MgS	MgSe	MgTe
Bandgap (eV), GGA	4.361	3.388	2.585	2.361
$P_{\rm r} (\mu C/cm^2)$	70	54	50	43
N _{site}	12	4	4	4
Energy above Hull (meV)	29	7	42	0
Number of phases below the FE phase	5	1	2	0
Barrier height (meV/f.u.)	198 (fixed) 189(relaxed)	343 (fixed) 65(relaxed)	360(fixed) 90(relaxed)	392 (fixed) 162(relaxed)
Piezoelectric modulus (C/m²)	2.61	0.48	0.46	0.27

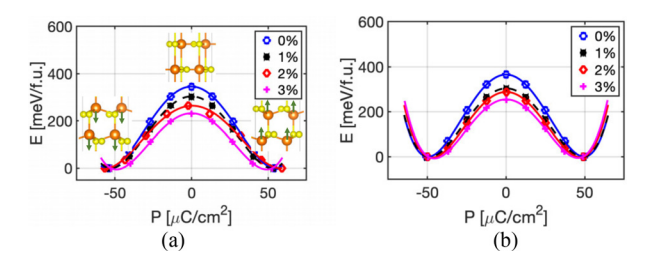


FIG. 5. Energy vs polarization in the FE switching path for (a) MgS and (b) MgSe with different biaxial tensile strain values of 0%, 1%, 2%, and 3%. The inset of (a) shows the structures, and arrows illustrate atom movement in FE switching. The unit cell sizes are set to be fixed throughout the switching path in the NEB simulation.

w-MgS and w-MgSe. The two minimum energy points have opposite electric polarization with a magnitude of approximately $50\mu\text{C/cm}^2$. The kinetic path of ferroelectric switching in the lattice is identified as the two sublattice atoms vertically move against each other. The top of the energy barrier point corresponds to a centrosymmetric structure. The switching barrier computed from the NEB simulations with GGA is 343 meV for MgS, 360 meV per switching atom for MgSe, and 392 meV for MgTe for a fixed size of the unit cell, as shown in Table I. Appling a biaxial strain in the horizontal hexagonal plane of the lattice lowers the barrier height. A 3% tensile strain lowers the barrier height to 230 meV and 250 meV for MgS and MgSe, respectively, whereas the polarization remains approximately unchanged. A similar trend is also observed for MgTe. Compared to the switching barrier height of \sim 200 meV per switching atom computed by using the same method for HfO₂, the switching barriers for magnesium chalcogenide FE materials are relatively high without strain, and the application of biaxial strain reduces the barrier height.

Furthermore, the FE switching barrier heights of magnesium chalcogenides can be reduced significantly, if the unit cell size is fully relaxed in the switching process, as shown in Fig. 6. For MgS, a local minimum point is developed at the centrosymmetric point, and the switching barrier height reduces to 65 meV. For MgSe, no local minimum point is developed, and the switching barrier height reduces to 90 meV. The switching is accompanied by an expansion of the inplane lattice constant of the hexagonal lattice structure, as also illustrated in Fig. 6. For MgTe, the switching barrier height reduces to 160 meV if the unit cell is fully relaxed in the FE switching process.

As also shown in Fig. 6, the lattice deforms considerably in the FE switching process of w-MgS and w-MgSe. To understand the large lattice deformation in the fully relaxed structure associated with

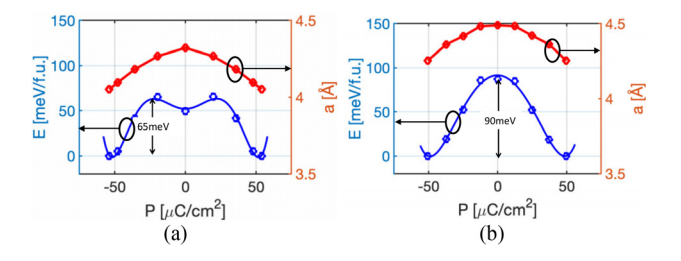


FIG. 6. Energy vs polarization in the FE switching path (left axis) and the in-plane lattice constant (right axis) in the FE switching path for (a) MgS and (b) MgSe. The unit cell is fully relaxed throughout the switching path in the NEB simulation.

ferroelectric switching of magnesium chalcogenide materials, their piezoelectric properties are compared. For non-centrosymmetric polar materials, a mechanical strain can induce ferroelectric polarization, and the ratio between the polarization and strain can be quantified by the piezoelectric tensor and modulus values, which are compared in Table I. The comparison indicates that the piezoelectric modulus of HfO₂ is over 5 times larger than that of either MgS or MgSe, and it is approximately an order of magnitude larger than that of MgTe. As a result, to induce a similar amount of polarization, a significantly large strain is necessary for the wurtzite magnesium chalcogenide materials, compared to FE HfO2. While the polarization values of magnesium chalcogenides are about 2/3 of that of HfO2, the much smaller piezoelectric modulus values of magnesium chalcogenides lead to significantly larger lattice distortion in the FE switching process, if the unit cells are fully relaxed. For the FE magnesium chalcogenide materials, the difference in the FE switching barrier heights between the fixed and fully relaxed unit cells is also considerably larger than that for FE HfO₂, as shown in Table I.

As a result, for device applications, the ferroelectric switching barrier height can be sensitive to the flexibility of the contact electrode material in a device with a magnesium chalcogenide layer sandwiched between two electrodes. For the FE layer between conventional metal electrodes that are not flexible, the deformation of the FE layer in the switching process is suppressed. On the other hand, if the electrode is flexible (e.g., with graphene or two-dimensional metallic materials, as recently demonstrated in a vertical van der Waals heterojunction ferroelectric tunnel junction device¹⁸) the electrode can be deformed in the FE switching process. In this case, the FE switching barrier height could be reduced significantly to facilitate FE switching.

It is noted that for porous and grained MgSe thin films, p-type conductivity has been reported, ^{19,20} which could be due to unintentional doping. While defects and doping effects need to be investigated in future experimental and theoretical studies, in the first step, we focus on the intrinsic properties of the materials here for materials screening and selection. Improvement of the material quality is likely to be necessary for the reduction of the leakage current due to unintentional doping, grain boundaries, and defects.

In summary, by using a comprehensive crystal selection algorithm, we identified a class of wurtzite materials that should have promising properties for ferroelectric applications, which include simple atomic structure, few crystals that are more stable, promising electronic bandgap, and appropriate barriers/polarization values. While AlN would need a third dopant to reduce the reversal barrier, 21,22 MgS, MgSe, and MgTe show a lower kinetic barrier for the polarization reversal, especially if there is an in-plane tensile strain from the electrodes or the electrodes are flexible.

J.G. acknowledges the support from National Science Foundation Award Nos. ECCS-1809770 and 1904580.

DATA AVAILABILITY

The data that support the findings of this study are available from the corresponding authors upon reasonable request.

REFERENCES

¹J. Müller, T. S. Böscke, U. Schröder, S. Mueller, D. Bräuhaus, U. Böttger, L. Frey, and T. Mikolajick, Nano Lett. 12, 4318 (2012).

- ²T. E. Smidt, S. A. Mack, S. E. Reyes-Lillo, A. Jain, and J. B. Neaton, Sci. Data 7, 72 (2020).
- ³K. F. Garrity, Phys. Rev. B **97**, 024115 (2018).
- ⁴G. Kresse and J. Furthmüller, Comput. Mater. Sci. 6, 15 (1996).
- ⁵H. J. Monkhorst and J. D. Pack, Phys. Rev. B 13, 5188 (1976).
- ⁶T. D. Huan, V. Sharma, G. A. Rossetti, and R. Ramprasad, Phys. Rev. B 90, 064111 (2014).
- ⁷Y. Wei, P. Nukala, M. Salverda, S. Matzen, H. J. Zhao, J. Momand, A. S. Everhardt, G. Agnus, G. R. Blake, P. Lecoeur, B. J. Kooi, J. Íñiguez, B. Dkhil, and B. Noheda, Nat. Mater. 17, 1095 (2018).
- ⁸S. E. Reyes-Lillo, K. F. Garrity, and K. M. Rabe, Phys. Rev. B **90**, 140103 (2014).
- ⁹T. Maeda, B. Magyari-Kope, and Y. Nishi, in IEEE International Memory Workshop (IMW) (2017), pp. 1–4.
- ¹⁰S. Clima, D. J. Wouters, C. Adelmann, T. Schenk, U. Schroeder, M. Jurczak, and G. Pourtois, Appl. Phys. Lett. **104**, 092906 (2014).
- ¹¹S. Clima, S. R. C. McMitchell, K. Florent, L. Nyns, M. Popovici, N. Ronchi, L. D. Piazza, J. Van Houdt, and G. Pourtois, in IEEE International Electron Devices Meeting (IEDM) (2018), pp. 16.5.1–16.5.4.
- ¹²J. Müller, T. S. Böscke, S. Müller, E. Yurchuk, P. Polakowski, J. Paul, D. Martin, T. Schenk, K. Khullar, A. Kersch, W. Weinreich, S. Riedel, K. Seidel, A. Kumar,

- T. M. Arruda, S. V. Kalinin, T. Schlösser, R. Boschke, R. van Bentum, U. Schröder, and T. Mikolajick, in IEEE International Electron Devices Meeting (2013), pp. 10.8.1–10.8.4.
- ¹³E. D. Grimley, T. Schenk, T. Mikolajick, U. Schroeder, and J. M. LeBeau, Adv. Mater. Interfaces 5, 1701258 (2018).
- ¹⁴W. Ding, Y. Zhang, L. Tao, Q. Yang, and Y. Zhou, Acta Mater. 196, 556 (2020).
- ¹⁵S. S. Fields, S. W. Smith, P. J. Ryan, S. T. Jaszewski, I. A. Brummel, A. Salanova, G. Esteves, S. L. Wolfley, M. D. Henry, P. S. Davids, and J. F. Ihlefeld, ACS Appl. Mater. Interfaces 12, 26577 (2020).
- ¹⁶ A. Jain, S. P. Ong, G. Hautier, W. Chen, W. D. Richards, S. Dacek, S. Cholia, D. Gunter, D. Skinner, G. Ceder, and K. A. Persson, APL Mater. 1, 011002 (2013).
- ¹⁷S. Fichtner, N. Wolff, F. Lofink, L. Kienle, and B. Wagner, J. Appl. Phys. **125**, 114103 (2019).
- ¹⁸J. Wu, H.-Y. Chen, N. Yang, J. Cao, X. Yan, F. Liu, Q. Sun, X. Ling, J. Guo, and H. Wang, Nat. Electron. 3, 466 (2020).
- ¹⁹ A. U. Ubale and Y. S. Sakhare, Mater. Sci. Semicond. Process. 16, 1769 (2013).
- ²⁰A. U. Ubale and Y. S. Sakhare, Vacuum **99**, 124 (2014).
- ²¹D. Jena, R. Page, J. Casamento, P. Dang, J. Singhal, Z. Zhang, J. Wright, G. Khalsa, Y. Cho, and H. G. Xing, Jpn. J. Appl. Phys., Part 1 58, SC0801 (2019).
- ²²S. Zhang, D. Holec, W. Y. Fu, C. J. Humphreys, and M. A. Moram, J. Appl. Phys. 114, 133510 (2013).